

General Disclaimer

One or more of the Following Statements may affect this Document

- This document has been reproduced from the best copy furnished by the organizational source. It is being released in the interest of making available as much information as possible.
- This document may contain data, which exceeds the sheet parameters. It was furnished in this condition by the organizational source and is the best copy available.
- This document may contain tone-on-tone or color graphs, charts and/or pictures, which have been reproduced in black and white.
- This document is paginated as submitted by the original source.
- Portions of this document are not fully legible due to the historical nature of some of the material. However, it is the best reproduction available from the original submission.



Waveform Inversion of Mantle Love Waves: the Born Seismogram approach

Toshiro Tanimoto

Seismological Laboratory
California Institute of Technology
Pasadena, California 91125

(NASA-CR-174483) WAVEFORM INVERSION OF
MANTLE LOVE WAVES: THE BORN SEISMOGRAM
APPROACH (California Inst. of Tech.) 44 p
HC A03/MF A01

N84-11622

Unclass

G3/46 42491

Abstract

Normal mode theory, extended to the slightly laterally heterogeneous Earth by the first-order Born approximation, is applied to the waveform inversion of mantle Love waves (200-500 sec) for the Earth's lateral heterogeneity at $l=2$ and a spherically symmetric anelasticity (Q_μ) structure. The data are from the Global Digital Seismograph Network (GDSN). The $l=2$ pattern is very similar to the results of other studies that used either different methods, such as phase velocity measurements and multiplet location measurements, or a different data set, such as mantle Rayleigh waves from different instruments. The results are carefully analyzed for variance reduction and are most naturally explained by heterogeneity in the upper 420 km. Because of the poor resolution of the data set for the deep interior, however, a fairly large heterogeneity in the transition zones, of the order of up to 3.5% in shear wave velocity, is allowed. It is noteworthy that Love waves of this period range can not constrain the structure below 420 km and thus any model presented by similar studies below this depth are likely to be constrained by Rayleigh waves (spheroidal modes) only.

The calculated modal Q values for the obtained Q_μ model fall within the error bars of the observations. The result demonstrates the discrepancy of Rayleigh wave Q and Love wave Q and indicates that care must be taken when both

Rayleigh and Love wave data, including amplitude information, are inverted simultaneously.

Anomalous amplitude inversions of G2 and G3, for example, are observed for some source-receiver pairs. This is due to multipathing effects. One example near the epicentral region, which is modelled by the obtained $l=2$ heterogeneity, is shown.

1. Introduction

Putting constraints on the lateral heterogeneity of the Earth is one of the most important contributions seismologists can make to the understanding of the dynamical behavior of the Earth. Since the work of Toksöz and Anderson (1966), most studies of the global scale heterogeneity of the upper mantle have used surface waves. The most recent contributions using this approach are by Nakanishi and Anderson (1983a, 1983b). Recently, Silver and Jordan (1981) and Masters *et al.* (1982) used standing wave analysis (free oscillations), which is, in essence, not so different from phase velocity measurements. In an entirely different approach, Woodhouse (1983) inverted the observed seismograms directly for the heterogeneity of the Earth. His result showed a pattern similar to that found by Masters *et al.* (1982). His derivations of the formula used for the inversion were quite complicated, however. Tanimoto (1983) showed that an application of the first order Born approximation to the conventional normal mode approach (Gilbert, 1970) gives equivalent formula. Recently, with a slightly simplified approach, Woodhouse and Dziewonski (1983) obtained a heterogeneous Earth model with the maximum angular order $l=8$, using probably the largest quantity of data so far.

In this paper, we apply the Born approximation method to mantle Love waves (200-500 sec) obtained from GDSN (Global Digital Seismographic Network) stations. We invert the seismograms directly for the lateral distribution of rigidity for different depths. The results are similar to those obtained by Masters *et al.* (1982), Woodhouse (1983), and Nakanishi and Anderson (1983a, 1983b). Considering the differences in the methods and/or the data, the similarity is quite remarkable. In the process of inversion, we also perturb the spherically symmetric anelasticity parameters Q_μ , because no recent Earth model adequately explains Love wave Q values. Most recent Q models are constructed for Rayleigh

wave Q, and there seems to be a yet unexplained difference between Rayleigh wave Q and Love wave Q at present.

We also show an interesting multipathing effect near the source region, which can be explained by the heterogeneity obtained.

2. Method

The equation of motion is given by

$$(\rho_0 + \delta\rho) \partial_t^2 u + (H_0 + H) u = f(t, x_s), \quad (1)$$

where the subscript 0 refers to the zeroth order spherically symmetric Earth, $\delta\rho$ and H are the deviations from it, and $f(t, x_s)$ is a source as a function of time t and position x_s . Tanimoto (1983) showed that, under the first order Born approximation, the seismograms in a slightly heterogeneous Earth can be written as

$$\begin{aligned} u = \text{Re} \sum_k \frac{e^{i\omega_k t}}{\omega_k^2} & \left[-\sum_m F_k^m \bar{u}_k^{(0)m} + \sum_{m'm} \frac{\bar{u}_k^{(0)m'} \langle km' | H | km \rangle F_k^m}{\omega_k^2} \right. \\ & + \sum_{s, k \neq s} \frac{1}{\omega_k^2 - \omega_s^2} \sum_{m'm} \left\{ F_s^m \bar{u}_k^{(0)m'} (\langle km' | H | sm \rangle - \omega_k^2 \langle km' | \delta\rho | sm \rangle) \right. \\ & \left. \left. + F_k^{m'} \bar{u}_s^{(0)m} (\langle sm | H | km' \rangle - \omega_k^2 \langle sm | \delta\rho | km' \rangle) \right\} \right] \quad (2) \end{aligned}$$

where $\bar{u}_k^{(0)m}$ is an eigenfunction of a k -th multiplet in the zeroth-order spherically symmetric Earth and satisfies

$$\rho_0 \omega_k^2 \bar{u}_k^{(0)m} = H_0 \bar{u}_k^{(0)m},$$

$$\langle km | \delta\rho | sm' \rangle = \int_E \delta\rho \bar{u}_k^{(0)m*} \bar{u}_s^{(0)m'} dV,$$

$$\langle km | H | sm' \rangle = \int_E \bar{u}_k^{(0)m'} H \bar{u}_s^{(0)m'} dV,$$

$$F_k^m = \int_E \bar{u}_k^{(0)m'} \bar{f}(p, x_g) dV,$$

and

$$\bar{\omega}_k^2 = \omega_k^2 + \frac{\sum_{m'm} \bar{u}_k^{(0)m'} (\langle km' | H | km \rangle - \omega_k^2 \langle km' | \delta\rho | km \rangle) F_k^m}{\sum_m \bar{u}_k^{(0)m} F_k^m}.$$

Here $\bar{f}(p, x_g)$ is the Laplace transformation of $f(t, x_g)$ with respect to time. This is equivalent to the formula derived by Woodhouse (1983) in a much more complicated way. The first term with the sum over m in $[\]$ represents a seismogram in a spherically symmetric Earth, and the rest are due to the lateral heterogeneity of the Earth. The second term in $[\]$ with the sum over m' and m is the contribution from the same multiplet k , and the rest, i.e. all terms in the second and the third lines, are the contribution from different multiplets $s (\neq k)$. Generally speaking, $\langle km' | H | sm \rangle$ and $\langle km' | \delta\rho | sm \rangle$ are much smaller than $\langle km' | H | km \rangle$ and $\langle km' | \delta\rho | km \rangle$. Thus the last terms are small unless $\omega_k \approx \omega_s$, that is when there exist modes with close eigenfrequencies. This condition is satisfied for the frequency range considered except for a few modes. For this reason, we drop the last terms in the following analysis, although it should be interesting to study these exceptional cases.

In the formal Born approximation approach, the second term is not exactly a contribution from the same multiplet k , but a contribution from modes with close eigenfrequencies. The last terms are contributions from modes with distant eigenfrequencies. If coupling of modes occur, (Luh, 1973, 1974; Woodhouse, 1980; Morris and Geller, 1982; Tanimoto and Bolt, 1983; Masters *et al.*, 1983), it should be included in the second term. Summation must be extended to other

- 6 -

multiplets in addition to the k -th one in such a case. Formally, the applicability of Born approximation approach is controlled by the magnitude (smallness) of terms associated with H and $\delta\rho$ compared with terms in the zeroth-order spherically symmetric Earth. However, in the following applications in this paper, the coupling effects are ignored.

In the geometrical optics approximation, Jordan (1978) showed that the frequency shift of the multiplet is the average of the local perturbation to the eigenfrequency over the great circular path. Similar proof can be established for attenuation in the same manner, i.e. the Q of the multiplet is the average of the local perturbation to the attenuation over the great circular path. Since this is not related to other topics in this paper, it is shown in the Appendix.

We find it convenient to change from epicentral coordinate, as in (2), to geographic coordinate, as Woodhouse and Girnius (1982) did. Then after dropping the terms in the second and the third lines, (2) becomes

$$u = \text{Re} \sum_k \frac{e^{i\omega_k t}}{\omega_k^2} \left(\sum_m R_k^m S_k^m - \frac{1}{\omega_k^2} \sum_{m'm} R_k^{m'} H_k^{m'm} S_k^m \right), \quad (3)$$

where

$$R_k^m = \sum_{N=-1}^1 \bar{u}_k^{(0)N} Y_l^{Nm}(\theta, \varphi),$$

$$S_k^m = - \sum_{N=-2}^2 F_k^N Y_l^{Nm}(\theta, \varphi)$$

and

$$Y_l^{Nm}(\theta, \varphi) \equiv P_l^{Nm}(\cos\theta) e^{im\varphi}$$

is the generalized spherical harmonics of Phinney and Burridge (1973). Here θ and φ are colatitude and longitude in the spherical coordinate and the

expressions for F_k^N are given in Woodhouse and Girnius (1982).

Computation of $Y_l^{Nm}(\theta, \varphi)$ is done by using the recursive relation for P_l^{Nm} , which is

$$P_l^{Nm} = -a_m P_l^{N, m+2} - b_m P_l^{N, m+2}$$

with

$$a_m = \sqrt{\frac{(l+m+2)(l-m-1)}{(l+m+1)(l-m)}}$$

and

$$b_m = \frac{2}{\sqrt{(l+m+1)(l-m)}} \left\{ \frac{(m+1)\cos\theta - N}{\sin\theta} \right\}$$

The recursion is started from $m=l$, noting

$$P_l^N(\cos\theta) = (-1)^{l-N} \sqrt{\frac{(2l)!}{(l+N)!(l-N)!}} \left(\cos\frac{\theta}{2}\right)^{l+N} \left(\sin\frac{\theta}{2}\right)^{l-N}.$$

This can be found in Edmonds (1960), whose notation is $d_{Nm}^k(\theta)$ instead of $P_l^{Nm}(\cos\theta)$.

Complete expressions for $H_k^{m'm}$ are given in Woodhouse and Dahlen (1978) in the absence of coupling effects. In our particular case, this becomes

$$\begin{aligned} H_k^{m'm} = & \left[\frac{m}{l(l+1)} \Omega + \alpha \varepsilon_n w_k \left\{ 1 - \frac{3m^2}{l(l+1)} \right\} \right] \delta_{m'm} \\ & + \sum_s \gamma_s^{m'm} \int_0^a M_s \delta \mu_s^{m'm} r^2 dr, \end{aligned} \quad (4)$$

where Ω is the sidereal rotation rate, 7.292115×10^{-5} (1/s), $\alpha \varepsilon_n$ is the ellipticity splitting parameter for a given multiplet k (Dahlen, 1976; Woodhouse and Dahlen, 1978),

$$\gamma_s^{m'm} = (-1)^{m'}(2l+1) \sqrt{\frac{2s+1}{4\pi}} \begin{pmatrix} l & s & l \\ 0 & 0 & 0 \end{pmatrix} \begin{pmatrix} l & s & l \\ -m' & m' & -m & m \end{pmatrix},$$

a the radius of the Earth, $\delta\mu_s^{m'-m}$ the spherical harmonic expansion of aspherically distributed rigidity (the angular order S, the azimuthal order $m'-m$), and

$$2\omega M_s = \left\{ l(l+1) - \frac{1}{2}s(s+1) \right\} \left(\frac{\partial w}{\partial r} - \frac{w}{r} \right)^2 + \left[l(l+1) \left\{ l(l+1) - 2 \right\} - \frac{1}{2}s(s+1) \left\{ 4l(l+1) - s(s+1) - 2 \right\} \right] \frac{w^2}{r^2},$$

where $\begin{pmatrix} l & s & l \\ 0 & 0 & 0 \end{pmatrix}$ is the Wigner's 3j symbol (e.g. Edmonds, 1960) and w is an eigenfunction of a torsional mode. We used the eigenfunctions of 1066A in this study (Gilbert and Dziewonski, 1975).

The first term in (4) is the contribution from rotation, the second from the hydrostatic ellipticity, and the third from aspherical distribution of rigidity. We dropped the density perturbation and the boundary perturbations in this study. We subtract the synthetic seismograms for the reference spherically symmetric Earth (1066A) with the rotation and ellipticity effects from the data and invert the resultant disturbances for $\delta\mu_s^{m'-m}$.

We found, however, that amplitudes were not fitted very well if we use the recently published Q models. This is not surprising, since most Q models are constructed in order to satisfy Q of Rayleigh waves and there seems to exist, at least at present, an inconsistency between Love wave Q and Rayleigh wave Q. Thus we adopted the Q model of Masters *et al.* (1983) as the starting model and perturbed them. Partial derivatives of the seismograms with respect to the intrinsic Q_μ are easily obtained, since Q^{-1} of surface waves are linear functionals of $Q_\mu^{-1}(r)$ (Anderson and Archambeau, 1964).

In the radial direction, we use two shells, one between the surface and 420 km and the other between 420 km and 670 km. In each shell, we solve for $\delta\mu_0^0, \delta\mu_2^0, \delta\mu_2^1, \delta\mu_2^2$, and $\delta q_m (= \delta(1/Q_m))$. Thus in total we have 14 parameters. Conventional least-squares is used in solving this.

3. Data

We analyzed Love waves from 11 large earthquakes in 1980 recorded by GDSN stations. A list of earthquakes and the source parameters used are given in Tables 1a and 1b. We used the source parameters determined by Nakanishi and Kanamori (1983) and did not perturb them during the inversion, since Love waves can place only four independent constraints on moment tensors.

In order to reduce the size of the data set, the seismograms were filtered between 2 mHz (500 sec) and 5 mHz (200 sec) and resampled at 40 sec intervals. A cosine taper was applied between 2 and 3 mHz and also between 4 and 5 mHz. An example of the data set for the earthquake in northern California (No. 24 in Table 1a) is shown in Fig. 1. G1 is not used in the analysis, and if G2 and G3 were clearly recorded the data were analyzed further. Fig. 1 shows some of the best examples in our data set. In many seismograms, glitches were present and the seismograms had to be truncated. In total, we found 60 source-receiver pairs with excellent S/N ratios. The great circle paths are shown in Fig. 2.

4. Analysis

First, we calculate partial derivatives of seismograms with respect to $\delta q (= \delta(1/Q))$ and $\delta\mu_l^m$ for each source-receiver pair. Equation (3) can be written symbolically as

$$u = u_0 + \sum_l \frac{\partial u_0}{\partial q_l} \delta q_l + \sum_l \sum_m \frac{\partial u_0}{\partial \mu_l^m} \delta \mu_l^m \quad (5)$$

where the subscript l refers to the shell number in the radial direction and $\delta\mu_l^m$ is the (l,m) component of spherical harmonic expansion of $\delta\mu$.

Instead of solving for complex $\delta\mu_l^m$, which is the case when we use complex spherical harmonics $Y_l^m(\theta, \varphi)$, we changed to $P_l^m(\cos\theta) \cos m\varphi$ and $P_l^m(\cos\theta) \sin m\varphi$ at this stage. Formulation up to this point is done by $Y_l^m(\theta, \varphi)$ of Edmonds (1960). It is advantageous to use them in the formulation, since we can fully use the properties of 3j symbols, but in computation real quantities are much easier to handle. We normalize the associated Legendre polynomial by $\left[(2-\delta_{m0})(2l+1)(l-m)! / (l+m)! \right]^{1/2}$ and use the notation $P_l^m(\cos\theta)$.

Fig. 3a shows an example of a set of partial derivatives for one source-receiver pair. The earthquake in Fig. 3 is No. 1 in Table 1a, and the receiver is ZOBO in Bolivia. All fundamental, first overtone, and second overtone modes between the periods of 200 sec and 500 sec are included in these calculations. This is the most time-consuming step in the inversion, taking about 20 hours on the VAX 11/780 computer.

In Fig. 3a, we show the data, the synthetic seismogram with ellipticity and rotation corrections, their differences, partial derivative with respect to $1/Q$ in the upper 420 km and that in the transition zone and partial derivatives with respect to corresponding spherical harmonic components of rigidity in the upper 420 km and those in the transition zone. Four large amplitude wave packets are G2, G3, G4 and G5 from left to right. The small amplitude oscillations in between are contributions from overtones. Contributions of overtones are larger in the deeper transition zone than in the upper 420 km, but in both shells, the fundamental modes are dominant. Fig.3b is the case of a different source-receiver pair, which shows the same features. From these two figures, we expect that results are mostly determined by fundamental modes.

The form of the problem becomes

$$A x = b \quad (6)$$

where the elements of A are given by $\frac{\partial u}{\partial q_i}$ and $\frac{\partial u}{\partial \delta \mu_i^0}$,

$$x^T = (\delta q_1, \delta q_2, \delta \mu_0^0, \dots)$$

and the elements of b are given by $u - u_0$ at each sampled point in the seismograms. Simple least squares method is used to estimate x, i.e.

$$x = (A^T A)^{-1} A^T b \quad (7)$$

Standard error of i-th parameter in x, σ_i , is estimated by

$$\sigma_i = \sqrt{\frac{(A^T A)^{-1}_{ii}}{n-m} \sum_{l=1}^n (\sum_k a_{lk} x_k - b_l)^2} \quad (8)$$

where $(A^T A)^{-1}_{ii}$ is the i-th diagonal element of $(A^T A)^{-1}$, n the number of data points, m the number of parameters used for fitting, and a_{lk} , x_k , and b_k are elements of A, x, and b.

5. Results

Heterogeneity

We performed inversions for five cases as shown in Table 2. The cases differ in whether Q is included and whether rigidity in the upper region (0-420 km) and/or in the lower region (420-670 km) are included. In the table, o means that the parameter is included, while x denotes that it is not. When Q is included, Q_μ in both the upper and the lower regions are perturbed. We calculated the variances for the initial model (spherically symmetric Earth with

rotation and ellipticity correction), σ_1^2 , and for the resultant model, σ_2^2 . Variance reductions are $(\sigma_1^2 - \sigma_2^2) / \sigma_1^2$ and are tabulated in Table 2.

Two features of this table deserve particular attention. First, as comparisons of 1(42.6%) with 2(42.2%) and 3(21.7%) with 4(21.2%) make clear, the interaction of the perturbation in the lower region achieves only an extremely small improvement in variance reduction. Second, incorporating Q in the inversion produces large variance reductions. This point is discussed in the next section.

Inverted results for the upper region are shown in Fig. 4 for each case. Coefficients of $l=2$, used for plotting, are given in Tables 3a and 3b. The chain and dashed lines correspond to positive and negative regions, respectively, and the solid line is the zero line. The contour interval is 0.4% in this figure. The similarity of the four figures suggests that the results of the aspherical distribution of $\delta\mu$ in the upper region are almost independent of the introduction of Q and also the lower region in the inversion. Only slight shifts of the patterns are observed. The coefficients of $l=2$ are tabulated in Table 3 with the estimated standard error for each case of inversion.

It is interesting to note, however, that case 5, in which all lateral heterogeneity is confined to the transition zone, gives smaller but comparable variance reductions (19.1%). The results are shown in Fig. 5, along with the results of cases 1 and 3 for the lower region. The results of case 5 display a very similar pattern to the results in the upper mantle shown in Fig. 4, but contour intervals are 5 times larger (2%). The peak value, $\delta\mu$ is about 7 %, as compared to about 1.5 % in Fig.4. This can be understood from Figs 3a and 3b. Partial derivatives for the lower region have virtually the same patterns as those for the upper region, but the amplitudes are about 5 times smaller. This is also the reason that the extra variance reductions achieved for cases 1 and 3 are so small compared to cases 2 and 4. Since the shapes of the partial derivatives are similar,

the extra degrees of freedom introduced into the model space by the introduction of parameters in the lower region are very small. And since the amplitudes are 5 times smaller, the extra variance reductions are very small.

This can possibly be avoided by using deep earthquakes, because as shown in Figs 3a and 3b the amplitudes of partial derivatives due to overtones tend to be greater for the lower region than for the upper region, which is opposite to the trend of fundamental modes. Thus, for deep earthquakes, the shapes of the partial derivatives can be different for different depths. The earthquakes in this paper, unfortunately, are all from shallow depths. Naturally, the resolution of our data set in the lower region is not good and our data set does not require lateral heterogeneity in the transition zone. But at the same time it can not rule out the possibility of a heterogeneous transition zone (420-670 km).

Fig. 6 compares the results in the upper region in case 1 with the results of Nakanishi and Anderson (1983) and Woodhouse (1983). The results of Nakanishi and Anderson are for Love wave phase velocities at the period of 307 seconds, which corresponds approximately to the dominant periods in our data set. The results of Woodhouse (1983) are obtained from Rayleigh waves using IDA (International Deployment of Accelerographs) network. Considering the differences in methods (waveform matching and phase velocity measurements) and in data (Love waves from GDSN and Rayleigh waves from IDA), the similarity of the results is quite remarkable. The results of Masters *et al.* (1982), which uses yet another approach (multiplet location measurements), also show a very similar pattern. We should note, however, that the interpretation of the depth of heterogeneity is different among these studies. Masters *et al.* (1982), for example, interpret their results entirely in terms of heterogeneity in the transition region.

Attenuation

The results for Q_u are discussed here. In Table 4, the initial model (Masters *et al.*, 1983) and the results of this study are shown. Differences between them are quite large, which confirms nothing but the inconsistency of Rayleigh wave and Love wave Q values. Most recent Q models are constructed mainly from Rayleigh wave (spheroidal mode) data. This is important because of its implication that simultaneous waveform inversion of Rayleigh and Love wave data has to be done with care. A Q model that fits Rayleigh wave data will give systematically higher amplitudes for Love waves and vice versa.

Q of torsional modes for case 1 are calculated and shown in Fig. 7 with observed torsional Q values reported in a table of PREM (Dziewonski and Anderson, 1982). The error bars are for observed Q values as reported there. The symbols \circ and \times correspond to calculated fundamental and first overtone modes. Q values of fundamental modes are rather low, while those of first overtones are not. Overall, Q values obtained in this study are consistent with reported Q values in PREM.

There is one caution, however. The source parameters are determined by Rayleigh waves using a certain Q structure (Nakanishi and Kanamori, 1983). Estimated moments depend upon the Q model. Since those moments are used in the process of inversion, there can be some trade-off between them. The fact that 60 paths for 11 earthquakes are used may have helped to reduce the trade-off, but there can still remain a systematic bias in estimated Q values.

6. Discussion

Figs. 8, 9, and 10 show the comparisons of waveforms before and after the inversion in case 1. In each figure, the top seismogram is the data; the second the synthetic seismogram for 1066A with the Q model of Masters *et al.* (1983) and the rotation and ellipticity correction; the third the same with the top one (the data); and the fourth the synthetic seismogram for our laterally heterogeneous Earth model.

Fig. 8 shows an interesting multipathing effect. The earthquake is No. 24 in Table 1a and the receiver is in Albuquerque, New Mexico (U.S.A.). Since the receiver is close to the source (about 15°), G2 and G3 and also G4 and G5 arrive at the receiver closely in time. The interesting feature in the data is the larger amplitude of G3 than that of G2, which is not modelled in the spherically symmetric Earth. However, this feature is explained in the seismograms after the inversion. Thus the obtained $l=2$ heterogeneity is capable of producing this multipathing effect, although the heterogeneity is not so strong. This is because the receiver is close to the source, where the effect of heterogeneity appears strongly. This should also be true for receivers near anti-podes, but there were no anti-podal data in our data set.

Fig. 9 shows the seismogram at Albuquerque for earthquake No. 8. This seismogram also has G2 and G3 in the first wave packet and G4 and G5 in the second wave packet. In this case, the main improvement is due to anelasticity.

Fig. 10 shows the worst example in the inversion. The source is No. 4 in the Kuril Islands, and the receiver is in India. The fit of the seismogram clearly became worse after the inversion. In particular, the arrival of the wave packet is too slow and is apparently perturbed in the wrong direction by the heterogeneous model. In order to see the point, the time interval from left to right is taken to be 4 times as large as that in Figs. 8 and 9. This is presumably because

$l=2$ heterogeneity is not enough to represent the Earth's heterogeneity. $L=2$ heterogeneity should be large, since fairly large variance reductions are achieved and the fit of the synthetic seismograms to the data is improved in most seismograms. However, an example like Fig. 10 shows that spherical components of lateral heterogeneity for $l \neq 2$ should counteract $l=2$ heterogeneity for some source-receiver pairs.

Although we do not discuss this problem extensively, there may be a problem of aliasing. This problem arises because of the existence of short wavelength heterogeneity in the Earth. When the maximum l in the inversion is not high enough, these short wavelength oscillations can affect the estimation of low order coefficients. There does not seem to be a simple cure for this problem, as long as spherical harmonic approach is used. We will address this problem in a later contribution.

7. Conclusion

Using mantle Love waves from the GDSN network, we obtained the lateral heterogeneity of $l=2$ pattern and spherically symmetric Q_μ by waveform inversion. Partial derivatives are calculated by using the first Born approximation to the normal mode approach. The obtained $l=2$ pattern is very similar to the results of Masters *et al.* (1982; multiplet location measurements), Woodhouse (1983; waveform inversion of Rayleigh waves from the IDA network), and Nakanishi and Anderson (1983; phase velocity measurements). Our results can most naturally be explained by heterogeneity in the upper 420 km. Because of the poor resolution in the transition zone, the data allow fairly large heterogeneity, of the order of 3.5% in shear wave velocity, in this region.

Q_μ structure is simultaneously inverted, and a reasonable model, which explains the observed Q of torsional modes, is obtained. However, possibility

of bias due to the trade-off between the Q structure and the estimated moments of the earthquakes remains. It is important to include Q in the inversion since no recent Q model satisfy torsional modes and a fairly large additional variance reduction is achieved by incorporating them. This result confirms the inconsistency of Rayleigh wave Q and Love wave Q values. Thus care must be taken in performing waveform inversion of Rayleigh waves and Love waves simultaneously.

Observed multipathing near the source is quite well modelled by the $l=2$ heterogeneity obtained in this study. But there are a few examples in which the fit of the synthetic seismograms becomes worse. This simply means that the Earth's heterogeneity is more complicated than $l=2$ pattern obtained.

Acknowledgement

I would like to thank Ichiro Nakanishi for discussions and suggestions in the course of this study. I also thank Don L. Anderson, Hiroo Kanamori, and Rob Comer for reading the manuscript and offering suggestions. This research was supported by NASA grant NSG-7610 and NSF grant EAR811-5236. Contribution number 3996, Division of Geological and Planetary Sciences, California Institute of Technology, Pasadena CA 91125.

Appendix: Q of a multiplet is the average of the local perturbation to the attenuation over the great circular path

The relation between the eigenfrequency of a multiplet in a heterogeneous Earth, $\bar{\omega}_k$, and that in a zeroth-order spherically symmetric Earth, ω_k , is given by

$$\bar{\omega}_k = \omega_k + \frac{\sum_{m'm} \bar{u}_k^{(0)m'} (\langle km' | H | km \rangle - \omega_k^2 \langle km' | \delta \rho | km \rangle) F_k^m}{2\omega_k \sum_m \bar{u}_k^{(0)m} F_k^m} \quad (A-1)$$

Attenuation can be incorporated in this formula by treating the elastic constants κ and μ in H as complex. We write $\bar{\omega}_k$ as

$$\bar{\omega}_k(\Theta, \Phi) = \omega_k + \lambda_k(\Theta, \Phi) + i\Lambda_k(\Theta, \Phi), \quad (A-2)$$

where (Θ, Φ) is the pole of the great circular path under consideration.

Jordan(1978) introduced the quantity, $\delta\omega_{\text{local}}(\Theta, \Phi)$, which is the local perturbation to the eigenfrequency, and defined it by

$$\delta\omega_{\text{local}}(\Theta, \Phi) = \int_0^a M^k(r) \delta m(r, \theta, \varphi) r^2 dr, \quad (A-3)$$

where δm is the perturbation of elastic constants and M^k the corresponding kernels. Then he showed

$$\lambda_k(\Theta, \Phi) \approx \sum_{s=2, \text{ even}}^l P_s(0) \sum_{t=-s}^s (\delta\omega_{\text{local}})_s^t Y_s^t(\Theta, \Phi) \quad (A-4)$$

where

$$\delta\omega_{\text{local}}(\theta, \varphi) = \sum_s \sum_t (\delta\omega_{\text{local}})_s^t Y_s^t(\theta, \varphi).$$

For attenuation, we define

$$\delta\omega^k(\theta, \varphi) = \int_0^a \left\{ K^k(r) \delta\kappa(r, \theta, \varphi) + U^k(r) \delta\mu(r, \theta, \varphi) \right\} r^2 dr \quad (A-5)$$

where $\delta\kappa$ and $\delta\mu$ are the imaginary parts of κ and μ , K^k and U^k are corresponding kernels. Note that the local Q value, $Q_{\text{local}}^k(\theta, \varphi)$, is given by

$$\frac{1}{Q_{\text{local}}^k(\theta, \varphi)} = \frac{2\delta\omega^k(\theta, \varphi)}{\omega_k}.$$

In exactly the same way as Jordan, we can obtain

$$\Lambda_k(\Theta, \Phi) \approx \sum_{s=2}^{2l} P_s(0) \sum_{t=-s}^s (\delta\omega^k)_s^t Y_s^t(\Theta, \Phi), \quad (A-6)$$

where

$$\delta\omega^k(\theta, \varphi) = \sum_s \sum_t (\delta\omega^k)_s^t Y_s^t(\theta, \varphi).$$

Using the relation (Backus, 1964, equation 44),

$$\frac{1}{2\pi a} \int_L Y_s^t(\theta, \varphi) ds = P_s(0) Y_s^t(\Theta, \Phi),$$

and extending the upper limit of the summation, $2l$, to infinity (geometrical optics approximation; Jordan, 1978), we obtain

$$\begin{aligned} \Lambda_k(\Theta, \Phi) &= \frac{1}{2\pi a} \int_L \delta\omega^k(\theta, \varphi) ds \\ &= \frac{\omega_k}{2} \frac{1}{2\pi a} \int_L \frac{ds}{Q_{\text{local}}^k(\theta, \varphi)} \end{aligned} \quad (A-7)$$

where $\int_L ds$ is the line integral along the great circular path. Q of a multiplet is related to Λ_k by

$$\Lambda_k(\Theta, \Phi) = \frac{\omega_k}{2Q_{\text{ave}}^k(\Theta, \Phi)},$$

thus we have

$$\frac{1}{Q_{\text{ave}}^k(\theta, \phi)} = \frac{1}{2\pi a} \int_L \frac{ds}{Q_{\text{local}}^k(\theta, \phi)} . \quad (\text{A-8})$$

Note that this is the relation between the standing wave Q (temporal Q) and for propagating wave Q (spatial Q), a factor of (group velocity)/(phase velocity) must be multiplied as weights.

REFERENCES

- Anderson, D. L. and Archambeau, C. B., 1964. The anelasticity of the Earth, *J. Geophys. Res.*, **69**, 2071-2084.
- Backus, G. E., 1964. Geographical interpretation of measurements of average phase velocities of surface waves over great circular and great semicircular paths, *Bull. seism. Soc. Am.*, **54**, 571-610.
- Dahlen, F. A., 1976. Reply, *J. Geophys. Res.*, **81**, 4951-4956.
- Dziewonski, A. M., and Anderson, D. L., 1981. Preliminary Reference Earth Model, *Phys. Earth Planet. Inter.*, **25**, 297-356.
- Edmonds, A. R., 1960. *Angular momentum in quantum mechanics*, Princeton University Press.
- Gilbert, F., 1970. Excitation of normal modes of the Earth by earthquake sources, *Geophys. J. R. astr. Soc.*, **22**, 223-226.
- Gilbert, F., and Dziewonski, A. M., 1975. An application of normal mode theory to the retrieval of structural parameters and source mechanism from seismic spectra, *Phil. Trans. R. Soc. Lond. A*, **278**, 187-269.
- Jordan, T. H., 1978. A procedure for estimating lateral variations from low-frequency eigenspectra data, *Geophys. J. R. astr. Soc.*, **52**, 441-455.
- Luh, P. C., 1973. Free oscillations of the laterally inhomogeneous Earth: Quasi degenerate multiplet coupling, *Geophys. J. R. astr. Soc.*, **32**, 187-202.
- Luh, P. C., 1974. Normal modes of a rotating, self-gravitating, inhomogeneous Earth, *Geophys. J. R. astr. Soc.*, **38**, 187-224.
- Masters, G., Jordan, T. H., Silver, P. G., and Gilbert, F., 1982. Aspherical earth structure from fundamental spheroidal-mode data, *Nature*, **298**, 609-613.
- Masters, G., Park, J., and Gilbert, F., 1983. Frequency shifts and amplitude variations in aspherically coupled multiplets, submitted to *J. Geophys. Res.*
- Morris, S. P., and Geller, R. J., 1982. Toroidal modes of a simple laterally

- heterogeneous sphere, *Bull. Seism. Soc. Am.*, 72, 1155-1166.
- Nakanishi, I., and Anderson, D. L., 1983a. Measurements of mantle wave velocities and inversion for lateral heterogeneity and anisotropy, Part I: Analysis of Great Circle Phase Velocities, submitted to *J. Geophys. Res.*
- Nakanishi, I., and Anderson, D.L., 1983b. Measurements of mantle wave velocities and inversion for lateral heterogeneity and anisotropy, Part II: Analysis by the single-station method, submitted to *Geophys. J. R. astr. Soc.*
- Nakanishi, I., and Kanamori, H., 1983. Source mechanisms of twenty-six large shallow earthquakes ($M_s > 6.5$) during 1980 from P-wave first motion and long-period Rayleigh wave data, submitted to *Bull. Seism. Soc. Am.*
- Phinney, R. A., and Burridge, R., 1973. Representation of the elastic-gravitational excitation of a spherical earth model by generalized spherical harmonics, *Geophys. J. R. astr. Soc.*, 34, 451-487.
- Silver, P. G., and Jordan, T. H., 1981. Fundamental spheroidal mode observations of aspherical heterogeneity, *Geophys. J. R. astr. Soc.*, 64, 605-634.
- Tanimoto, T., 1983. A simple derivation of the formula to calculate synthetic long-period seismograms in a heterogeneous Earth by normal mode summation, submitted to *Geophys. J. R. astr. Soc.*
- Tanimoto, T. and Bolt, B. A., 1983. Coupling of torsional modes in the Earth, *Geophys. J. R. astr. Soc.*, 74, 83-95.
- Toksöz, M. N., and Anderson, D. L., 1966. Phase velocities of long-period surface waves and structure of the upper mantle, I. Great-circle Love and Rayleigh wave data, *J. Geophys. Res.*, 71, 1649-1658.
- Woodhouse, J. H., 1980. The coupling of nearly resonant multiplets in the Earth's free oscillation spectrum, *Geophys. J. R. astr. Soc.*, 61, 261-283.
- Woodhouse, J. H., 1983. The joint inversion of seismic waveforms for lateral variations in Earth structure and earthquake source parameters, in+

Proceedings of the Enrico Fermi International School of Physics, LXXXV
(H. Kanamori and E. Boschi, eds.), North Holland, in press.

Woodhouse, J. H., and Dahlen, F. A., 1978. The effect of a general aspherical perturbation on the free oscillations of the Earth, *Geophys. J. R. astr. Soc.*, **53**, 335-354.

Woodhouse, J. H., and Dziewonski, A. M., 1983. Mapping the upper mantle: Three dimensional modelling of Earth structure by inversion of seismic waveforms, submitted to *J. Geophys. Res.*

Woodhouse, J. H., and Girnius, T. P., 1982. Surface waves and free oscillations in a regionalized earth model, *Geophys. J. R. astr. Soc.*, **68**, 653-673.

FIGURE CAPTIONS

Fig. 1: An example of filtered seismograms (2 - 5 mHz) for the earthquake No. 24 in Table 1a.

Fig. 2: Great circle paths of 60 source-receiver pairs.

Fig. 3a: An example of a set of the data and the partial derivatives for one source-receiver pair. The earthquake is No. 1 in Table 1a and the receiver is ZOBO in Bolivia. The top three traces are the observed data, the synthetic seismogram for the model 1066A with rotation and ellipticity correction and the residual between the two. The next two are the partial derivatives with respect to q ($= 1/Q$) in the upper 420 km and in the transition zone. The next six traces are the partial derivatives with respect to the spherical harmonic components of $\delta\mu$ in the upper 420 km. For example, (21C) denotes the coefficient of $P_2^1(\cos\theta) \cos\phi$. The last six traces are those for the transition zone.

Fig. 3b: Same as Fig. 3a except for a different source-receiver pair.

Fig. 4: The results of the inversion in the upper 420 km. The numbers on the top right corner correspond to the case in Table 2. $L=2$ components of $\delta\mu$ are plotted at an contour interval of 0.4 %. The dashed lines correspond to negative region, the chain lines to positive region and the solid lines are the zero lines. The negative peak is about 1.5 % both on the East Pacific Rise and India. In terms of shear wave velocity, this becomes about 0.7%.

Fig. 5: The results of the inversions for the transition zone. Note that the contour intervals are larger than those in Fig. 4.

Fig. 6: Comparison of the results of case 1 with the results of other studies. The second is Love wave phase velocity analysis by Nakanishi and Anderson (1983b) for the period of 307 sec. The third is the result of Woodhouse(1983), using a similar method but Rayleigh waves from IDA network.

Fig. 7: Computed torsional mode Q values for the inverted Q_μ model. The symbols o and x correspond to fundamental and first overtone modes. The symbols * with error bars are the observed torsional Q values found in Dziewonski and Anderson(1982).

Fig. 8: Comparison of the data and the synthetic seismograms before and after the inversion. The first and the third traces from top are the observed seismogram, the second the synthetic seismogram for 1066A with rotation and ellipticity correction, the fourth the the synthetic seismogram

for the obtained heterogeneous Earth. In this example, the receiver is close to the source (about 15 degrees), so the first wave packet contains both G2 and G3 and the second G4 and G5. Amplitude inversion of G2 and G3 is reproduced in the synthetic for the obtained heterogeneous model.

Fig. 9: Same as Fig.8 except for a different source receiver pair.

Fig. 10: The worst example in our inversion. Clearly, the wave packet is perturbed in the wrong direction by the obtained heterogeneity. This demonstrates a rather trivial point that the Earth's heterogeneity can not be represented accurately by $l=2$ term only.

Table 1a
List of Earthquakes (in 1980) Used

No.	m	d	h	m	s	Lat.	Lon.	Ms	Region
1	1	1	18	42	40.0	38.815N	27.780W	6.7	Azores
3	2	7	10	49	16.0	54.158S	158.890E	6.5	Macquarie Islands
4	2	23	5	51	3.2	43.530N	148.753E	7.0	Kurile Islands
7	3	24	3	59	51.3	52.969N	167.670W	6.9	Fox Islands
8	6	9	3	28	18.9	32.220N	114.985W	6.4	Cal-Mex Border
18	7	29	3	11	56.3	13.101S	166.338E	6.7	Vanuatu Islands
19	10	10	12	25	23.5	36.195N	1.354E	7.3	Algeria
24	11	8	10	27	34.0	41.117N	124.253W	7.2	N. California
26	11	23	18	34	53.8	40.914N	15.366E	6.9	Italy
27	12	17	16	21	58.8	49.479N	129.496W	6.8	Vancouver Island
28	12	31	10	32	11.0	46.060N	151.453E	6.5	Kurile Islands

Table 1b
Source parameters of the earthquakes used

No.	depth(km)	τ	$M_0(\times 10^{20})$	δ	λ	φ
1	9.75	17.2	2.38	86.2	3.0	-31.0
3	9.75	29.7	1.9	84.0	0.0	-70.0
4	43.0	19.3	6.31	70.0	89.2	27.0
7	33.0	30.1	2.95	60.0	88.1	53.3
8	9.75	15.4	0.465	90.0	180.0	140.1
16	43.0	19.1	1.57	54.0	93.5	160.0
19	9.75	30.2	4.89	54.0	81.8	225.0
24	16.0	31.7	10.3	90.0	0.0	49.8
26	9.75	44.7	2.84	63.0	275.8	-43.0
27	9.75	26.2	1.54	90.0	180.0	-37.1
28	33.0	27.8	2.90	68.0	89.6	28.3

KEY:

τ - rise time (sec)

M_0 - seismic moment (dyne cm)

δ - dip angle (deg)

λ - slip angle (deg)

φ - strike, measured clockwise from north (deg)

Table 2

Results of inversion for 5 cases with variance reductions

	1	2	3	4	5
Q	o	o	x	x	x
upper (0-420 km)	o	o	o	o	x
lower (420-670 km)	o	x	o	x	o
σ^2 reduction (%)	42.6	42.2	21.7	21.2	19.1

Table 3a

Results of the inversion for $l=2$ coefficients of $\delta\mu_l^m$.
Sigma (σ) is the standard error calculated from (8).

		case 1		case 2	
		$\delta\mu_l^m$	σ	$\delta\mu_l^m$	σ
Upper	20	0.118	0.068	0.045	0.017
	21C	0.152	0.027	0.107	0.007
	21S	-0.093	0.058	-0.196	0.015
	22C	0.606	0.043	0.615	0.011
	22S	-0.073	0.056	-0.353	0.014
	20	-0.397	0.353		
Lower	21C	-0.239	0.141		
	21S	-0.563	0.305		
	22C	0.045	0.223		
	22S	1.495	0.291		

Table 3b

		case 3		case 4	
		$\delta\mu_l^m$	σ	$\delta\mu_l^m$	σ
Upper	20	-0.042	0.079	-0.079	0.020
	21C	0.114	0.032	0.108	0.008
	21C	-0.068	0.068	-0.191	0.017
	22C	0.639	0.050	0.618	0.012
	22S	-0.049	0.085	-0.351	0.017
Lower	20	-0.203	0.411		
	21C	-0.037	0.165		
	21S	-0.667	0.356		
	22C	-0.110	0.260		
	22S	-1.612	0.340		
		case 5			
		$\delta\mu_l^m$	σ		
Lower	20	-0.336	0.106		
	21C	0.525	0.042		
	21S	-0.977	0.090		
	22C	3.104	0.066		
	22S	-1.832	0.087		

Table 4

Starting Q_μ model(Masters et al., 1983) and the inverted results

	Masters et al.(1983)	Case 1	Case 2
0 - 420 km	120	91 ± 1	91 ± 1
420 - 670 km	280	168 ± 20	163 ± 20
670 - 2887 km	340	Not perturbed	Not perturbed

ORIGINAL PAGE IS
OF POOR QUALITY

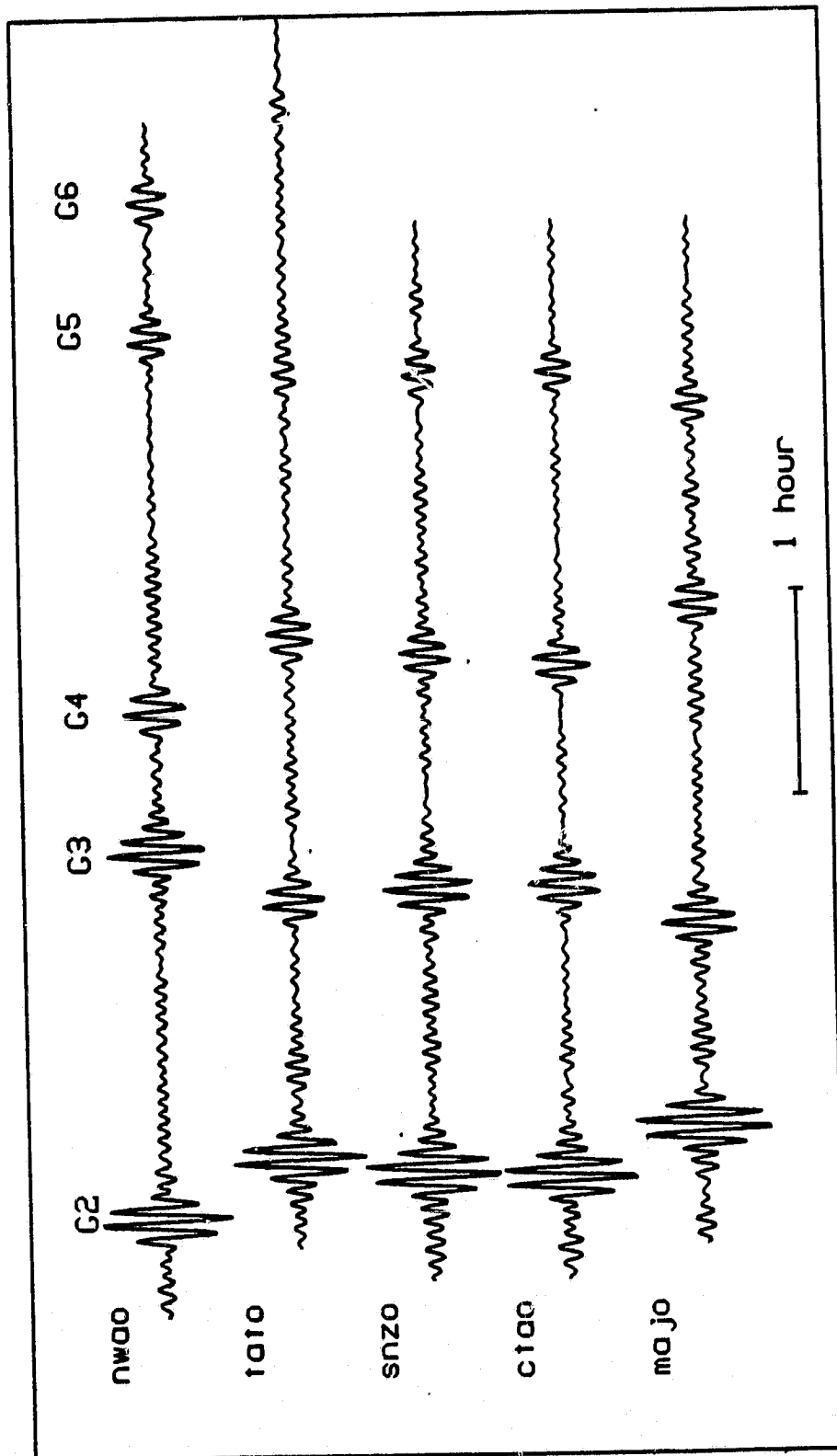


Fig. 1

ORIGINAL PAGE IS
OF POOR QUALITY

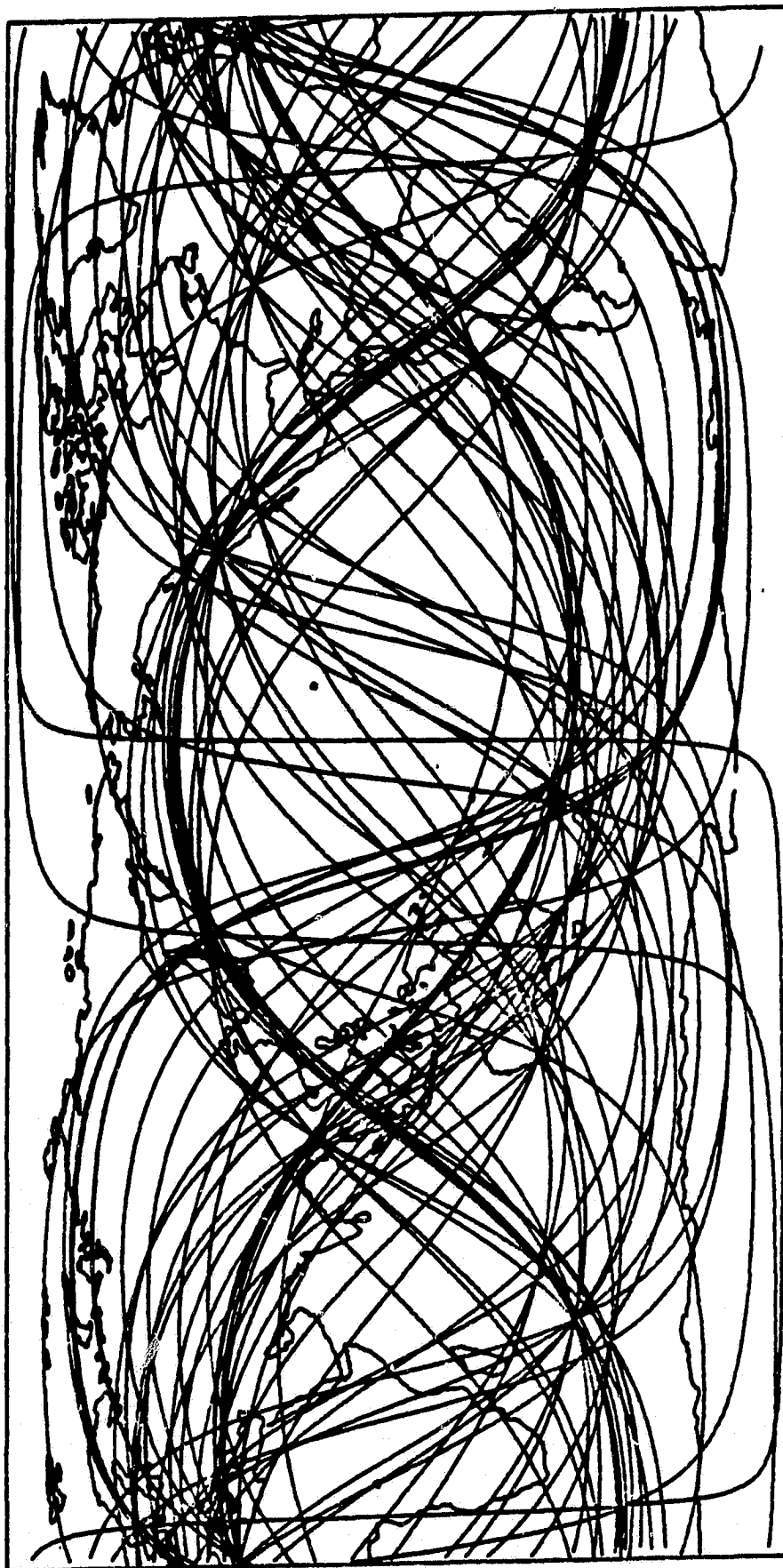



















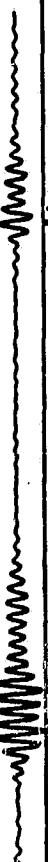
















Fig. 2

ORIGINAL PAGE IS
OF POOR QUALITY

A1 zobo			
DATA			830.84
SPHE. SYM.			709.64
RESIDUAL			473.12
du/dq1			56483.90
du/dq2			10959.90
0-420	0 0		39366.80
	2 0		4228.79
	2 1 C		20098.60
	2 1 S		12560.30
	2 2 C		8496.58
	2 2 S		17033.30
420-670	0 0		7559.61
	2 0		829.63
	2 1 C		3862.59
	2 1 S		2414.78
	2 2 C		1627.83
	2 2 S		3264.76

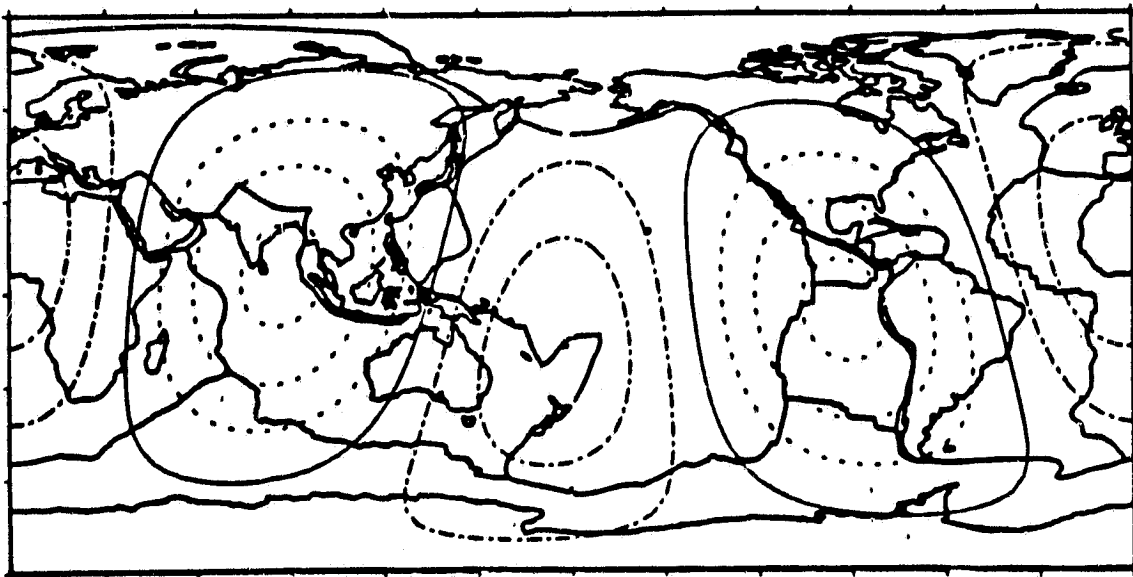
C24 anmo			
DATA			2148.05
SPHE. SYM.			1109.27
RESIDUAL			1904.35
du/dq1			96836.90
du/dq2			19325.90
0-420	0 0		63692.30
	2 0		28267.50
	2 1 C		37952.90
	2 1 S		20448.20
	2 2 C		35207.00
	2 2 S		12232.40
420-670	0 0		12257.80
	2 0		5852.90
	2 1 C		7362.26
	2 1 S		4244.43
	2 2 C		6811.06
	2 2 S		2495.70

ORIGINAL PAGE IS
OF POOR QUALITY

0 - 420 km

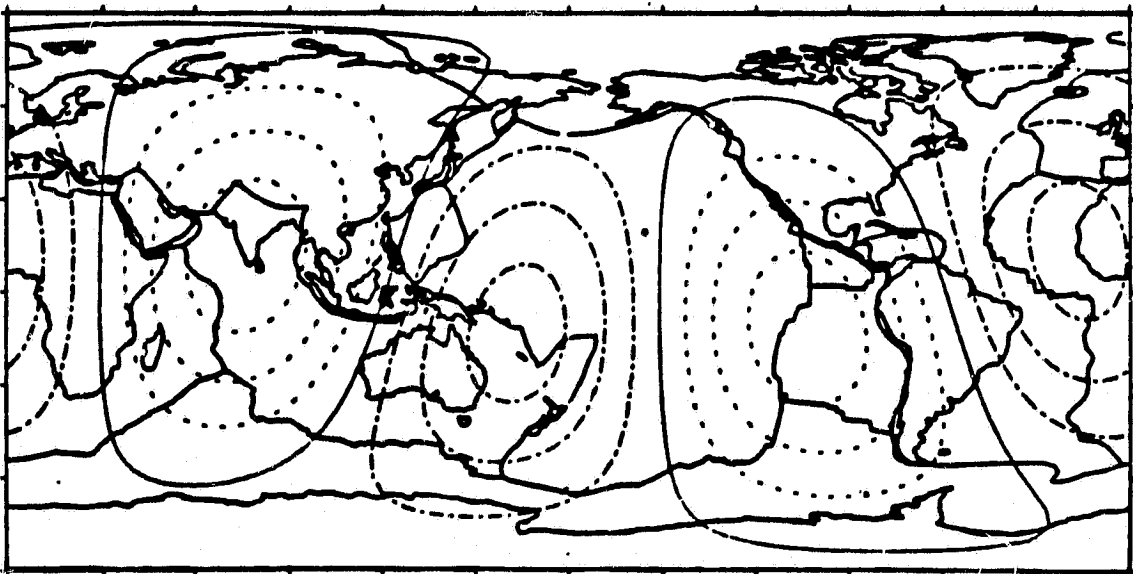
1

Contour 0.4 per cent



2

Contour 0.4 per cent

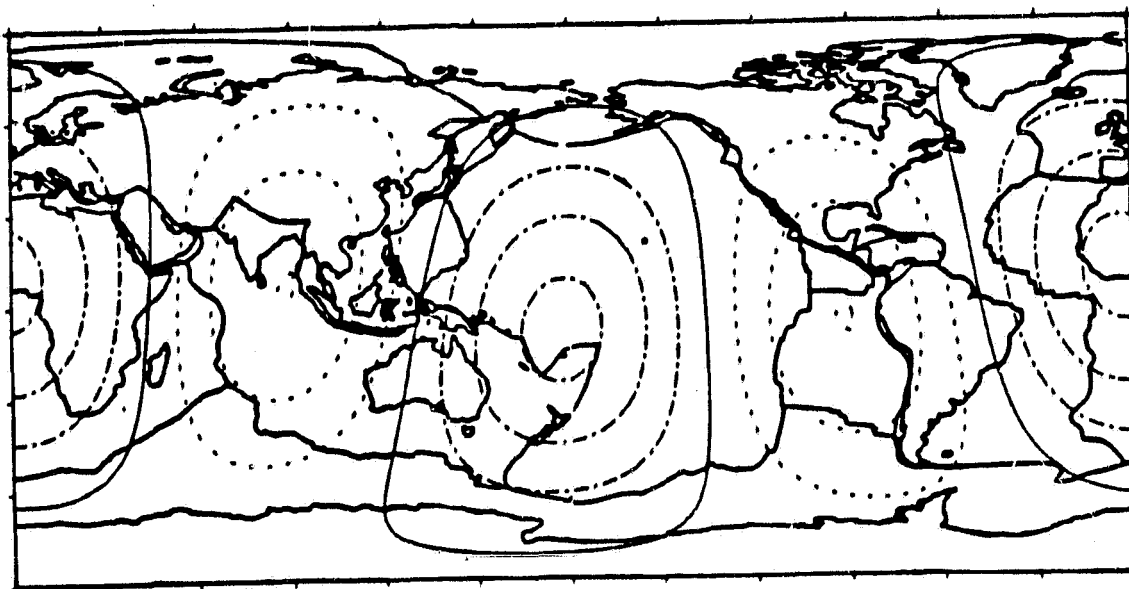


ORIGINAL PAGE IS
OF POOR QUALITY

0 - 420 km

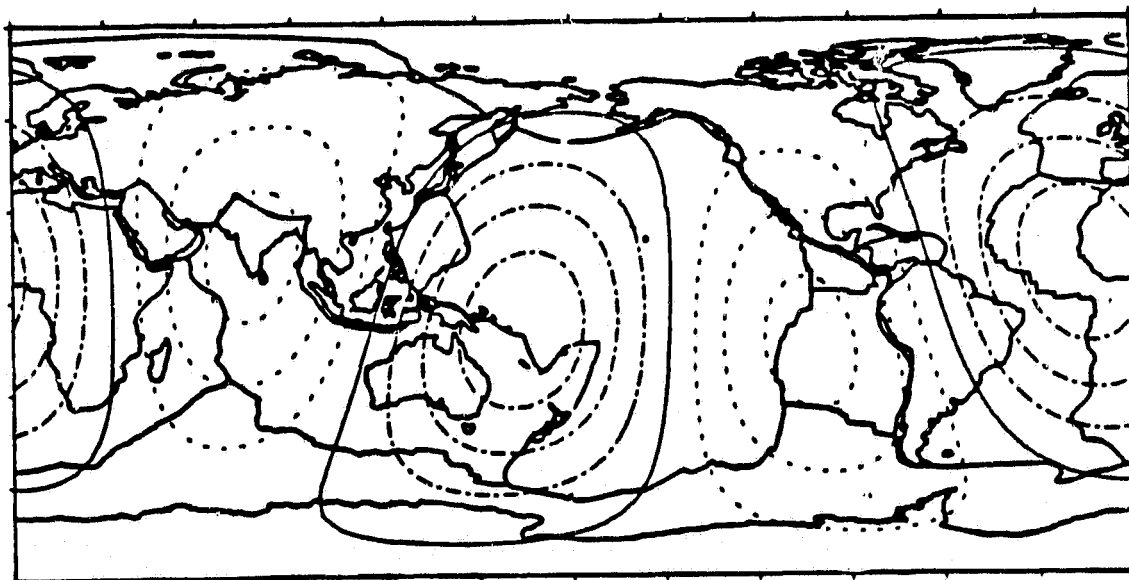
3

Contour 0.4 per cent



4

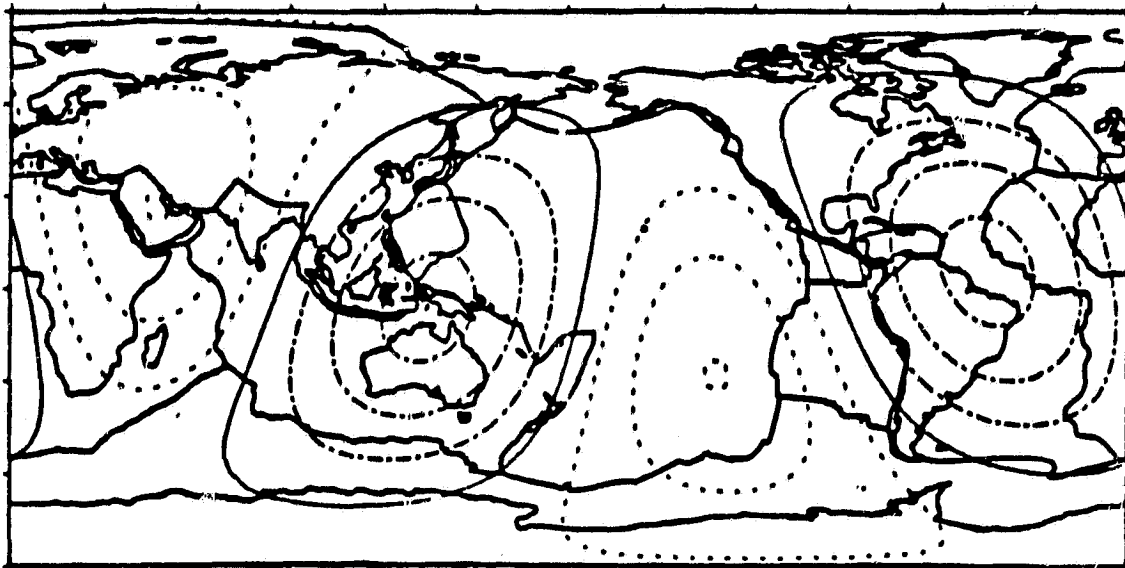
Contour 0.4 per cent



420 - 670 km

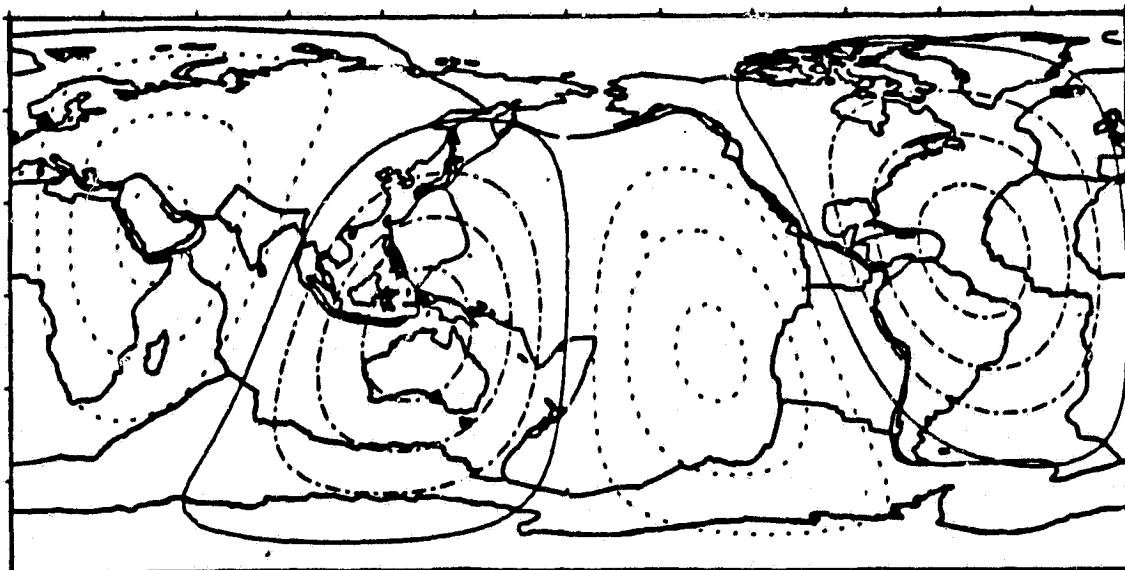
1

Contour 1.0 per cent



3

Contour 1.0 per cent



ORIGINAL PAGE 19
OF POOR QUALITY

420 - 670 km

5

Contour 2.0 per cent

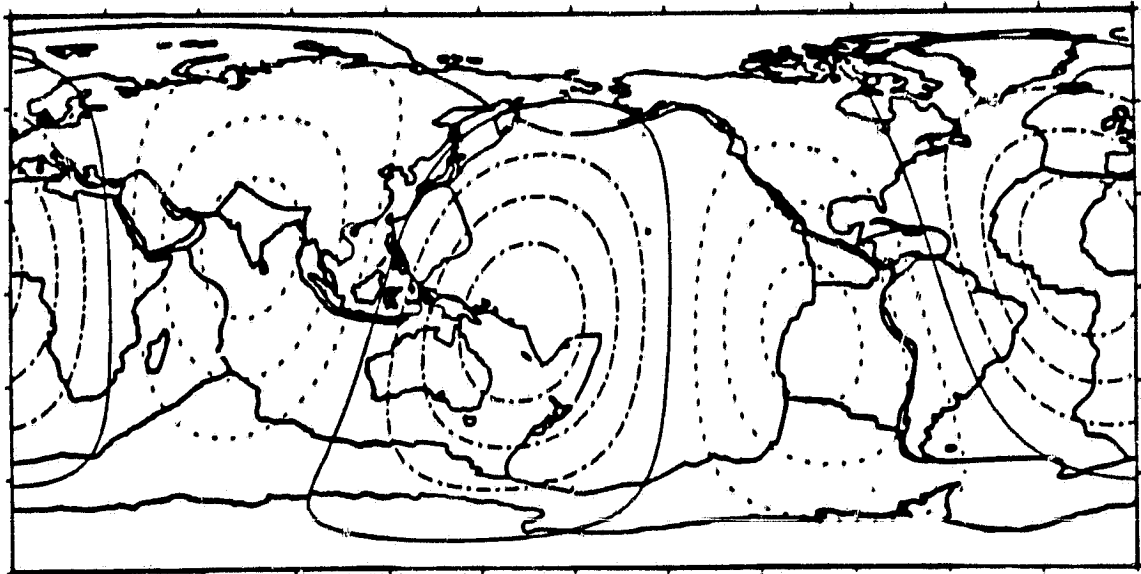
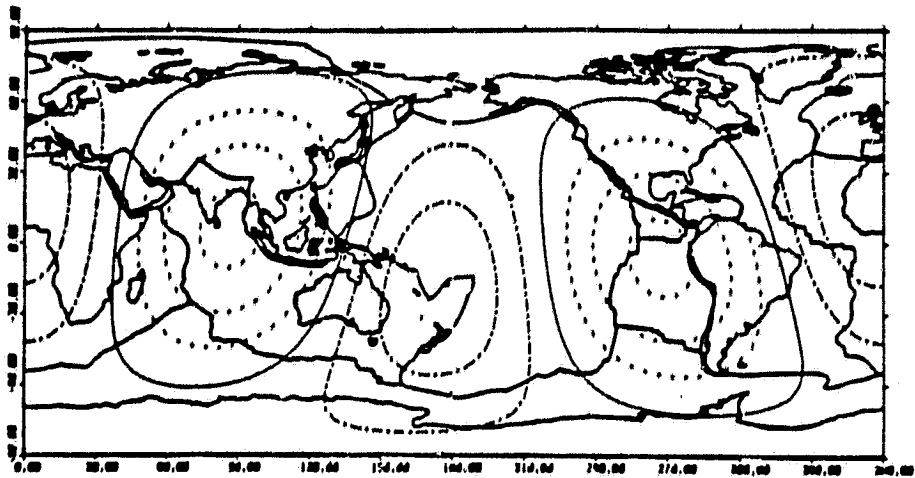
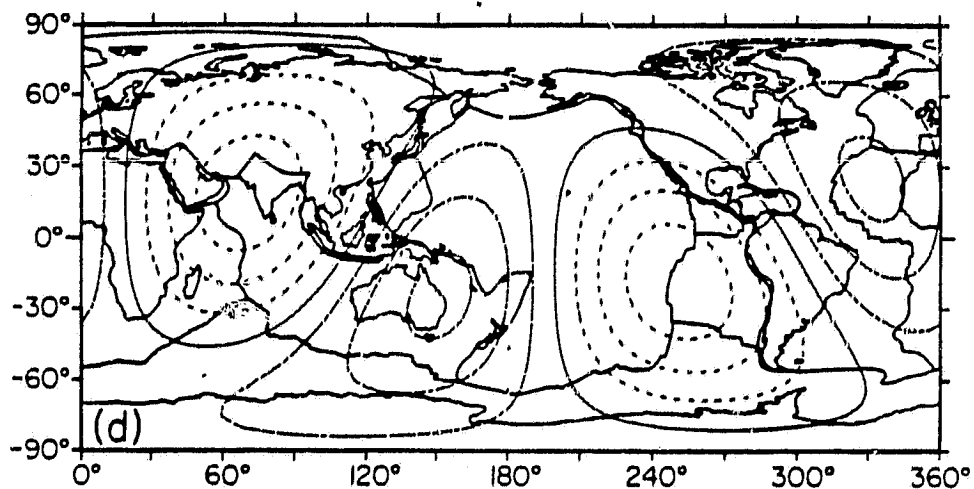


Fig. 5 A

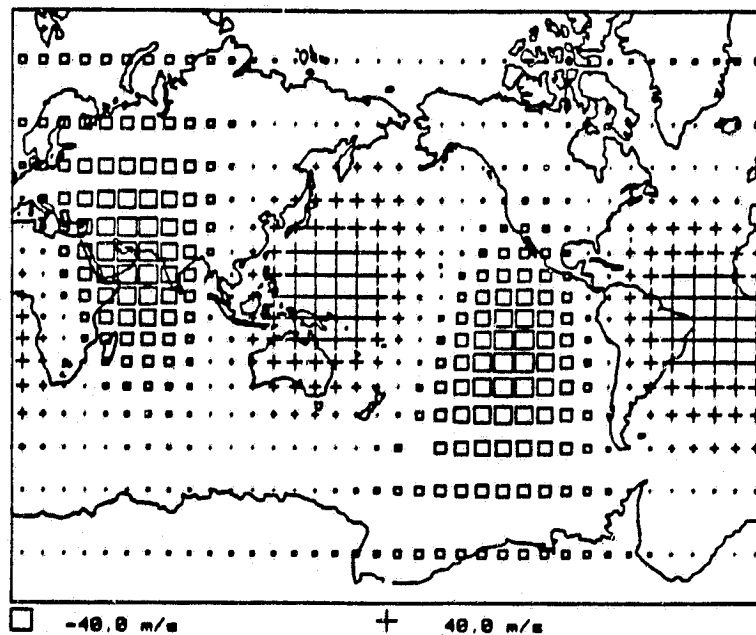
1 0 - 420 km Contour 0.4 %



T = 307 sec Contour 0.02 km/s



MEAN VELOCITY PERTURBATIONS IN THE DEPTH RANGE 13-378 KM



ORIGINAL PAGE IS
OF POOR QUALITY

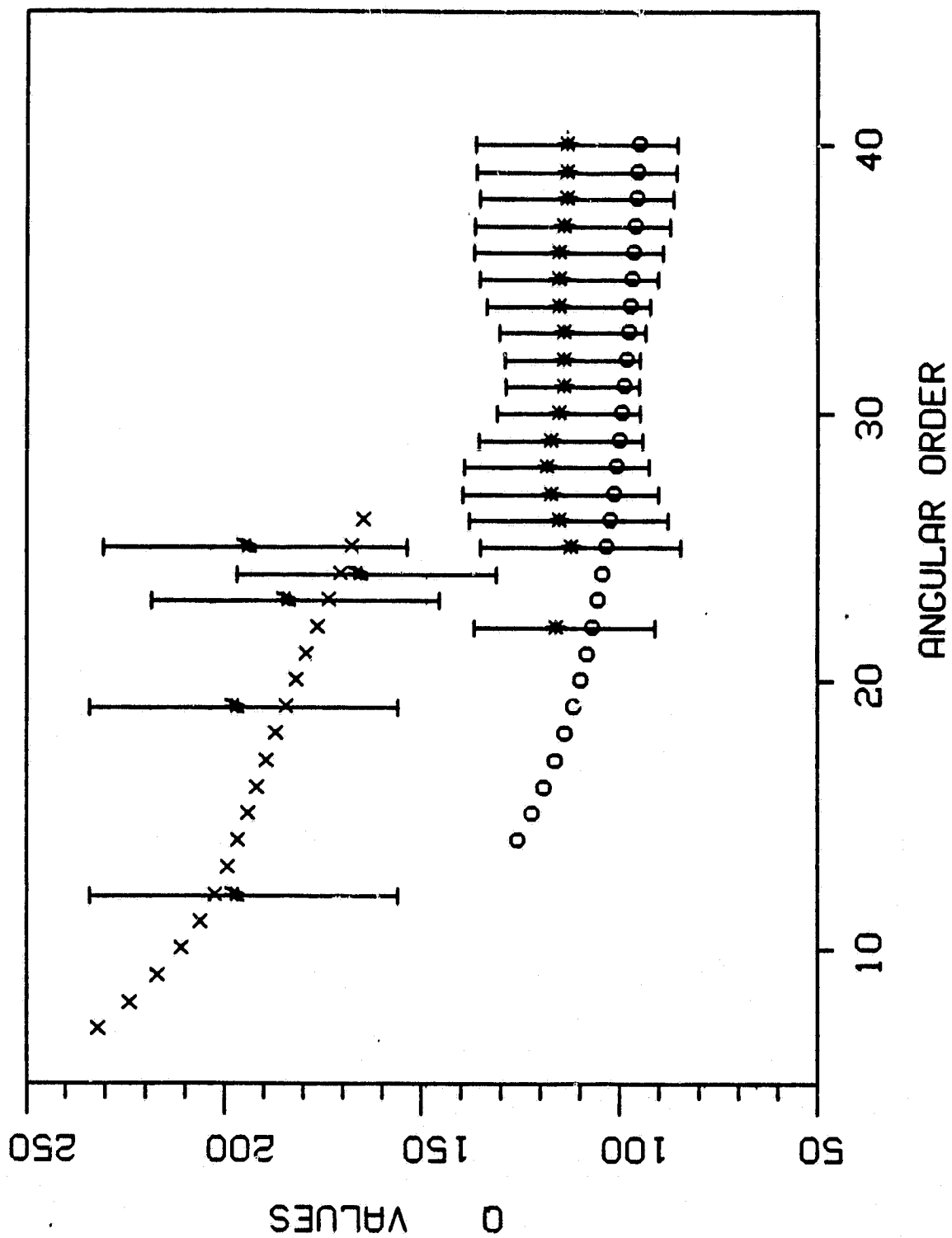
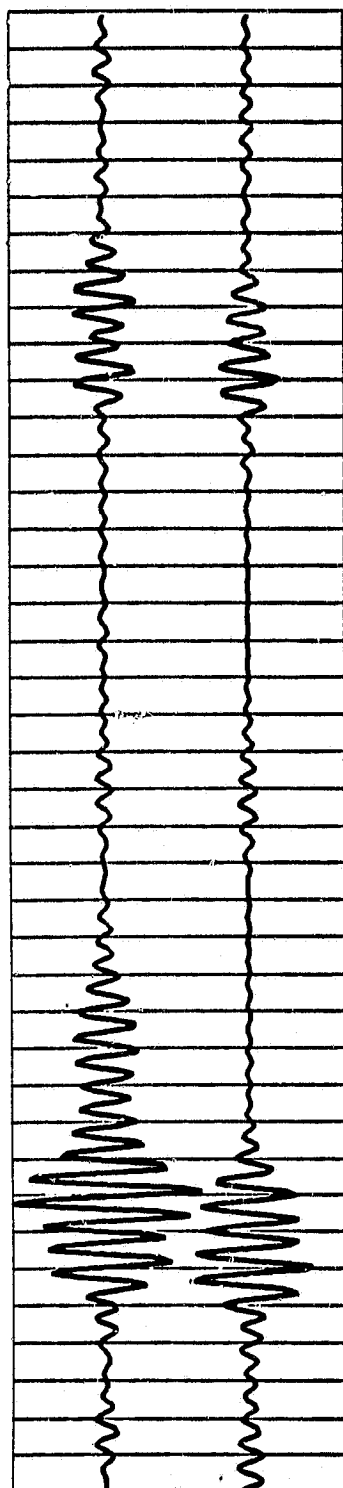
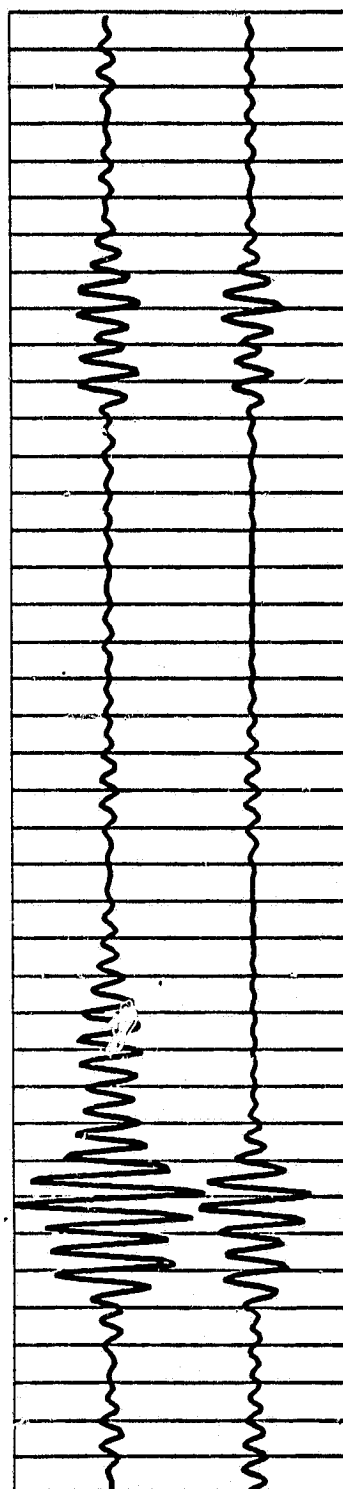


Fig. 7

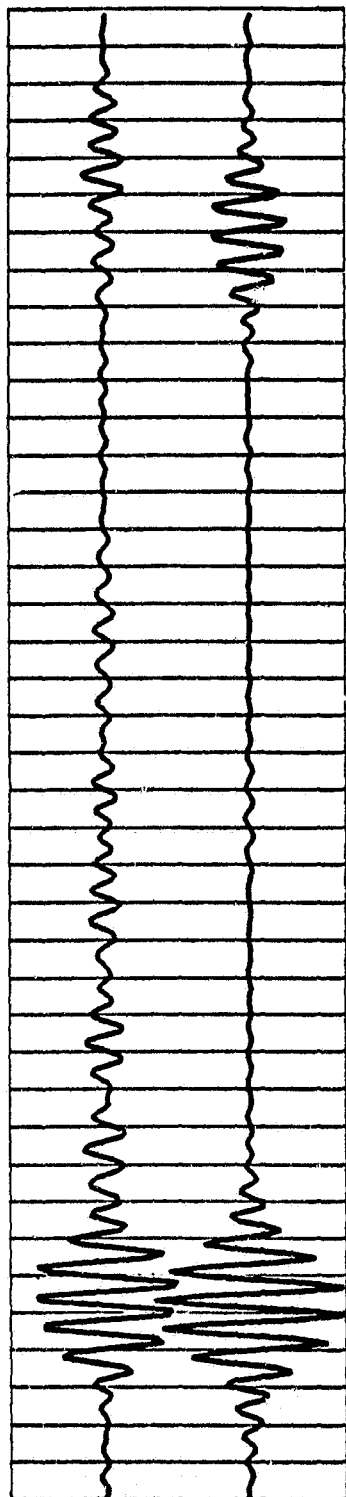
C24 anmo



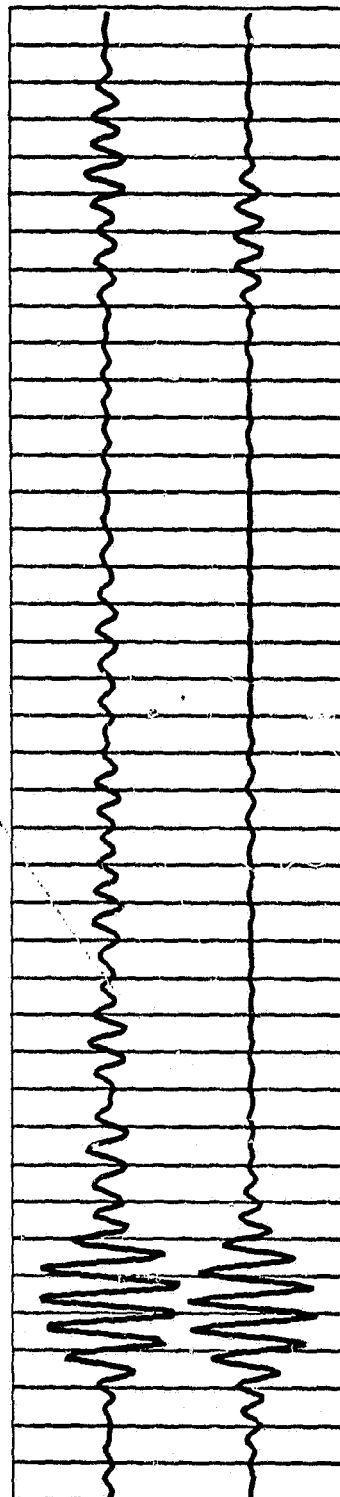
ORIGINAL PAGE IS
OF POOR QUALITY



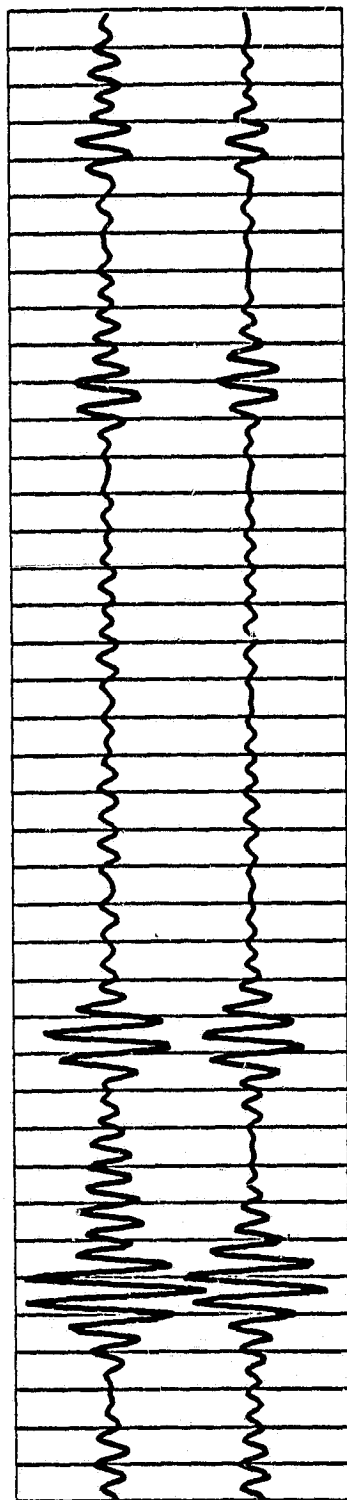
C8 anmo



ORIGINAL PAGE IS
OF POOR QUALITY



K4 shio



ORIGINAL PAGE IS
OF POOR QUALITY

